Visual Fatigue Relaxation for Stereoscopic Video via Nonlinear Disparity Remapping

Changjae Oh, *Student Member, IEEE*, Bumsub Ham, *Member, IEEE*, Sunghwan Choi, *Student Member, IEEE*, and Kwanghoon Sohn, *Senior Member, IEEE*

***Abstract*—A nonlinear disparity remapping scheme is presented to enhance the visual comfort of stereoscopic videos. The stereoscopic video is analyzed for predicting a degree of fatigue with the viewpoint of three factors: 1) spatial frequency; 2) disparity magnitude; and 3) disparity motion. The degree of fatigue is then estimated in a local manner. It can be visualized as an index map so-called a "visual fatigue map," and an overall fatigue score is obtained by pooling the visual fatigue map. Based on this information, a nonlinear remapping operator is generated in two phases: 1) disparity range adaptation and 2) operator nonlinearization. First, a disparity range is automatically adjusted according to the determined overall fatigue score. Second, rather than linearly adjusting the disparity range of an original video to the determined disparity range, a nonlinear remapping operator is constructed in a manner that the disparity range of inducible problematic region is compressed, while that of comfortable region is stretched. The proposed scheme is verified via subjective evaluations where visual fatigue and depth sensation are compared among original videos, linearly remapped videos, and nonlinearly remapped videos. Experimental results show that the nonlinearly remapped videos provide more comfort than the linearly remapped videos without losing depth sensation.**

***Index Terms*—Nonlinear disparity remapping, visual fatigue, visual fatigue map.**

I. Introduction

IN THESE days, stereoscopic videos have been widely prevailed and successfully commercialized thanks to their realistic three-dimensional (3D) effect. For giving an optimal 3D effect, viewing environments should be carefully considered when stereoscopic videos are produced. Otherwise, the 3D effect might become excessive or deficient, which induces human to have unsatisfactory experiences [1]. Visual fatigue is one of the most unsatisfactory experiences in viewing a stereoscopic video. Generally, it is caused by the conflict between vergence (convergence and divergence) and accommodation, since vergence changes along an object while accommodation is fixed to the display [2], [3]. Many researchers have investigated various factors inducing visual fatigue, such as spatial frequency, disparity magnitude, disparity motion, and disparity gradient [2]–[9].

The disparity range should be properly adjusted for the amount of depth perception being controlled in order to give satisfactory viewing experience [10]–[16]. Traditionally, a linear remapping scheme has been used to adjust disparity range homogeneously, the computational complexity of which is not expensive [10]. However, it might cause visual artifacts such as a cardboard cutout in that the relative depth of neighboring objects is likely to be flattened [17]. Recently, nonlinear disparity remapping schemes have been presented to reduce such artifacts while enhancing the 3D perception [10], [12], [14], [18]. However, most nonlinear disparity remapping methods have concentrated on elaborating the 3D perception rather than reducing visual fatigue. For example, most methods have handled visual fatigue by simply scaling a disparity range to the visual comfort zone [10], [14], [18].

In this paper, we propose a nonlinear disparity remapping scheme which considers visual fatigue factors existing in a stereoscopic video. To this end, visual fatigue is predicted by considering spatial frequency, disparity magnitude, and disparity motion. The predicted visual fatigue is presented as an index map, so called a "visual fatigue map," and an overall score is computed by pooling the visual fatigue map. The disparity range is automatically adjusted according to the overall fatigue score. Within this, a nonlinear remapping operator is constructed in a manner that the disparity range of inducible problematic region is compressed, and *vice versa*.

The remainder of the paper is organized as follows. Section II introduces related works for the disparity remapping. Then, the nonlinear disparity remapping scheme is described in Section III. In Section IV, experimental results of the proposed method and its comparison with state-of-the-art method are presented. Finally, we conclude the paper in Section V.

II. Related Works

A. Visual Fatigue in Stereoscopic Video

It has been found that viewing 3D contents is disturbed by various kinds of visual fatigue factors [2], [3], [7], [8], [19]-[21], of which conflict between vergence and accommodation of eyes is a well-known

Manuscript received October 4, 2013; revised December 24, 2014; accepted January 8, 2015. Date of publication March 2, 2015; date of current version June 4, 2015. This work was supported by the National Research Foundation of Korea (NRF) grant funded by the Korean Government (MSIP) under Grant NRF-2013R1A2A2A01068338.

C. Oh, S. Choi, and K. Sohn are with the School of Electrical and Electronic Engineering, Yonsei University, Seoul 120-749, Korea (e-mail: khsohn@yonsei.ac.kr).

B. Ham is with the Willow Team, Institut National de Recherche en Informatique et en Automatique (INRIA), Paris 75214 CEDEX 13, France.

Color versions of one or more of the figures in this paper are available online at http://ieeexplore.ieee.org.

Digital Object Identifier 10.1109/TBC.2015.2402471

problem [2], [19]–[21]. Such a conflict is unnatural status in human visual system, causing visual fatigue [3]. In addition, various visual fatigue factors have been investigated in terms of the characteristics of stereoscopic image [2], [3], [5], [7]–[9], [22]. It has been presented that the disparity magnitude is closely related to visual fatigue [2], [3], [22]. As the disparity magnitude becomes larger, conflict between vergence and accommodation becomes much severe, which in result causes visual fatigue. Thus, maximum disparity is generally constrained to one degree of angular disparity [3], [22], [23]. Object motion has also been known as one of the visual fatigue factors [3], [7]–[9]. Eyes become strained when the viewing object moves fast, since motion complexity is related to the temporal disparity change. In [3], it was shown that visual fatigue occurs when disparity motion is high, since temporal disparity change is related to linkage between vergence and accommodation. Spatial frequency also affects the visual fatigue [4], [5]. As spatial frequency becomes higher, binocular fusion ability decreases and it causes visual fatigue. In addition, the disparity gradient, i.e., difference of disparities between objects, has presented as a visual fatigue inducing factor. That is, the scene having a wide disparity range with multiple objects is hard to fuse simultaneously and causes visual fatigue, since disparity gradient exceeds a fusion limit [3], [24], [25].

Several visual fatigue prediction methods have been proposed to measure the degree of fatigue in an objective manner [5], [6], [9], [18], [26]. In [5], the degree of stereoscopic impairments was measured as a score, where shooting parameters and camera misalignment were estimated by image features. Choi *et al.* investigated various fatigue factors and determined the best model for fatigue prediction by using multiple regressions with subjective assessments [6]. Jung *et al.* exploited a motion of a salient object to construct visual comfort model [9]. Sohn *et al.* presented a visual fatigue prediction scheme by computing disparity gradient, between nearby objects and object thickness [26].

B. Disparity Remapping

A disparity remapping is one of the most essential post-production techniques since 3D effect is influenced by viewing environments such as a display size and a viewing distance. It solves such a problem by adapting a disparity range to the viewing environments. Traditionally, a linear remapping is used for the depth adjustment, which controls disparity range homogeneously [10], [18].

In order to perform the disparity remapping elaborately, various nonlinear remapping methods have been proposed to enhance depth perception while reducing depth distortion [10], [12]–[15]. Lang *et al.* presented nonlinear disparity remapping operators to enhance the depth perception of salient object [10]. A salient region was generated to capture visual attractiveness of the scene, and a nonlinear remapping operator was generated based on the importance of each disparity. Lin *et al.* proposed an optimization scheme through cropping and warping of a stereoscopic image pair to reduce the vertical disparity misalignment while enhancing depth perception [12]. Jung and Ko addressed a depth sensation problem by reflecting a behavior of human visual system [13]. Each disparity value was rescaled by optimizing energy models which consider a just noticeable depth difference. Yan *et al.* proposed a disparity remapping technique for reducing distortions of stereoscopic contents, where the relationship between neighboring features is preserved with line and plane bending constraints [14]. Recently, Sohn *et al.* presented a disparity remapping approach to reduce visual fatigue in a stereoscopic image, which is similar to the proposed method [15]. In [15], an iterative process finds an optimal disparity range of the stereoscopic image, and then the other iterative process compresses the disparity range of detected local fatigue region. In our work, the disparity remapping operator is generated automatically for each scene to handle temporal coherency between adjacent frames, which can be applied to the stereoscopic video.

III. Visual Fatigue Relaxation via Nonlinear Disparity Remapping

A. Overall System

The objective of the proposed disparity remapping scheme is to control the disparity range with respect to the predicted degree of fatigue. In other words, the proposed scheme relaxes the eye strain in fusing discomfortable objects. The overall process of the proposed method is shown in Fig. 1. In order to predict the degree of fatigue in a stereoscopic video, three factors are taken into account: spatial frequency, disparity magnitude, and disparity motion (Section III-B1). As an output of the visual fatigue prediction, a visual fatigue map is obtained, indicating the degree of fatigue in a local manner (Section III-B2). In addition, with the given visual fatigue map, an overall fatigue score can be obtained by pooling the visual fatigue map (Section III-B2). By using this information, the nonlinear disparity remapping operator is generated in two steps: the disparity range adaptation and operator non-linearization (Section III-C).

The disparity range is determined based on the overall fatigue score of the stereoscopic video. A threshold is set to decide whether the viewing condition of the stereoscopic video would be discomfortable or not. Based on the decision, the disparity range becomes smaller if the scene is determined to be discomfortable. In a comfortable video case, on the other hand, the disparity range is stretched within the pre-determined visual comfort range. Then, the remapping operator is non-linearized to adjust the disparity between objects by compressing the range of disparity within the problematic region, and *vice versa*. Assuming that similar objects are likely to have similar disparity, we can infer the degree of fatigue in each object by computing an average degree of fatigue for each disparity. Accordingly, disparity gradient can be adjusted with respect to the degree of fatigue. Furthermore, the proposed disparity remapping scheme considers temporal coherency by determining the disparity range and generating the operator for each scene.

By using the generated remapping operator, input disparity maps are remapped, and finally, the input stereoscopic video

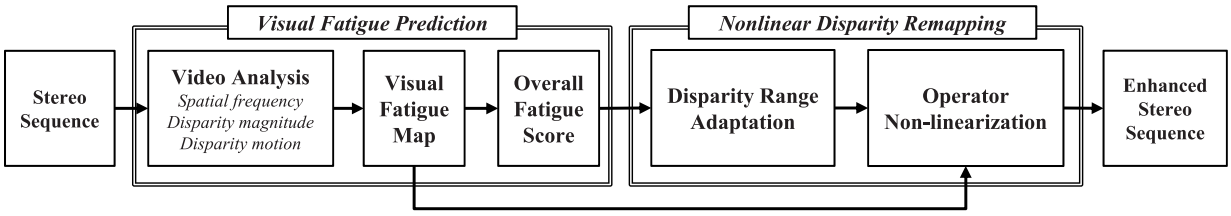

Fig. 1. Overview of the proposed disparity remapping scheme. With an input stereo sequence, visual fatigue is predicted and visual fatigue maps and an overall fatigue score are obtained. Nonlinear disparity remapping is then performed to adapt disparity range and relax visual fatigue.

is retargeted using remapped disparity maps by depth-image-based-rendering (DIBR) technique [27].

B. Visual Fatigue Prediction

Inspired by the previous studies [2]–[9], we present a visual fatigue prediction method using three fatigue inducing factors: the spatial frequency, the disparity magnitude, and the disparity motion. Each factor is presented as a visual fatigue model which captures the degree of fatigue in a local manner. Thus, it can be visualized as an index map indicating degrees of fatigue locally, *i.e.*, the intensity value of the index map is proportional to the degree of the predicted visual fatigue. A visual fatigue map is then generated via aggregating three fatigue models and an overall fatigue score is computed by a pooling strategy.

1) Visual Fatigue Factor Modeling:

a) Spatial frequency: We utilize the fact that an image with high spatial frequency gives more visual discomfort than that with low spatial frequency [4], [5]. Morrone and Burr presented that the important visual features are perceived at points where a local phase congruency has the maximum value [28]. In addition, Henriksson *et al.* concluded that human V1 cortex shows a phase-sensitive pooling of spatial frequency in natural images [29]. The phase congruency is thus exploited to extract the spatial frequency in the nature image [30]. Let $I_g(\mathbf{p}) : \Omega \rightarrow \mathbf{R}$ be an original image in grayscale where $\Omega \subset \mathbf{N}^2$ is an open and bounded space with 2D coordinate $\mathbf{p} = (x, y) \in \Omega$. The orientation angle of the filter denotes $\theta_k = k\pi/J$, $k = \{0, 1, \ldots, J-1\}$ where J is the number of orientations. By applying even- and odd-symmetric filters M_n^e and M_n^o with n scale, even and odd response vector $[e_{n,\theta_k}(\mathbf{p}), o_{n,\theta_k}(\mathbf{p})] = [I_g(\mathbf{p}) * M_n^e, I_g(\mathbf{p}) * M_n^o]$ can be obtained. Here, log-Gabor filter is exploited for M_n^e and M_n^o [28]. Then, the local amplitude can be computed as follows:

$$A_{n,\theta_k}(\mathbf{p}) = \sqrt{e_{n,\theta_k}^2(\mathbf{p}) + o_{n,\theta_k}^2(\mathbf{p})}. \tag{1}$$

Also, the local energy is computed as follows:

$$E_{\theta_k}(\mathbf{p}) = \sqrt{F_{\theta_k}^2(\mathbf{p}) + H_{\theta_k}^2(\mathbf{p})}, \tag{2}$$

where $F_{\theta_k}(\mathbf{p}) = \sum_n e_{n,\theta_k}(\mathbf{p})$ and $H_{\theta_k}(\mathbf{p}) = \sum_n o_{n,\theta_k}(\mathbf{p})$. Finally, the phase congruency at each pixel can be measured as follows:

$$PC(\mathbf{p}) = \frac{1}{Z_n} \cdot \frac{\sum_k E_{\theta_k}(\mathbf{p})}{\mu + \sum_n \sum_k A_{n,\theta_k}(\mathbf{p})}, \tag{3}$$

where μ and Z_n are a small positive constant and a normalization coefficient, respectively.

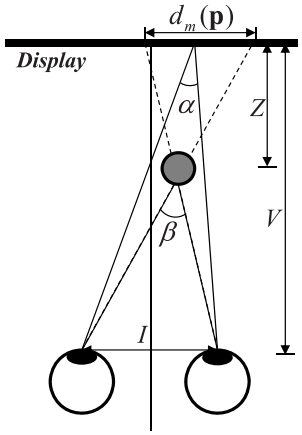

Fig. 2. Geometry of stereoscopic display system. Angular disparity can be computed by subtraction β from α.

b) Disparity magnitude: In stereoscopic images, there exists the visual comfort zone since accommodation of human eyes under natural viewing condition is limited [2], [3]. If the disparity between stereoscopic images increases over the visual comfort zone, eyes get strained due to the conflict between vergence and accommodation. Thus, a disparity magnitude is leveraged for penalizing the values over the threshold of the visual comfort zone.

Since the depth perception depends on the viewer's position, a display size, and an image resolution, the disparity expressed by displacement between pixels (image disparity) cannot show the relative score efficiently. Alternatively, angular disparity can be used to measure the human's perceived disparity by reflecting the specific viewing environments such as a viewing distance, a display size, and an inter-ocular distance.

As shown in Fig. 2, angular disparity is obtained by subtracting angle between two eyes and object (β) from angle between two eyes and display (α). To compute an angular disparity $d_a(\mathbf{p})$ by given an image disparity $d_c(\mathbf{p})$, it is needed to convert $d_c(\mathbf{p})$ into the real magnitude of the displayed disparity denoted as $d_m(\mathbf{p})$. With the assumption that the stereo images are rectified, $d_c(\mathbf{p})$ can be converted to $d_m(\mathbf{p})$ as follows:

$$d_m(\mathbf{p}) = \frac{X_m}{X_c} \cdot d_c(\mathbf{p}), \tag{4}$$

where X_c is the horizontal pixel size of the image, and X_m is the horizontal length of the display. Then, distance between an object and display Z is computed as follows:

$$Z = \frac{d_m(\mathbf{p}) \cdot V}{d_m(\mathbf{p}) - I}, \tag{5}$$

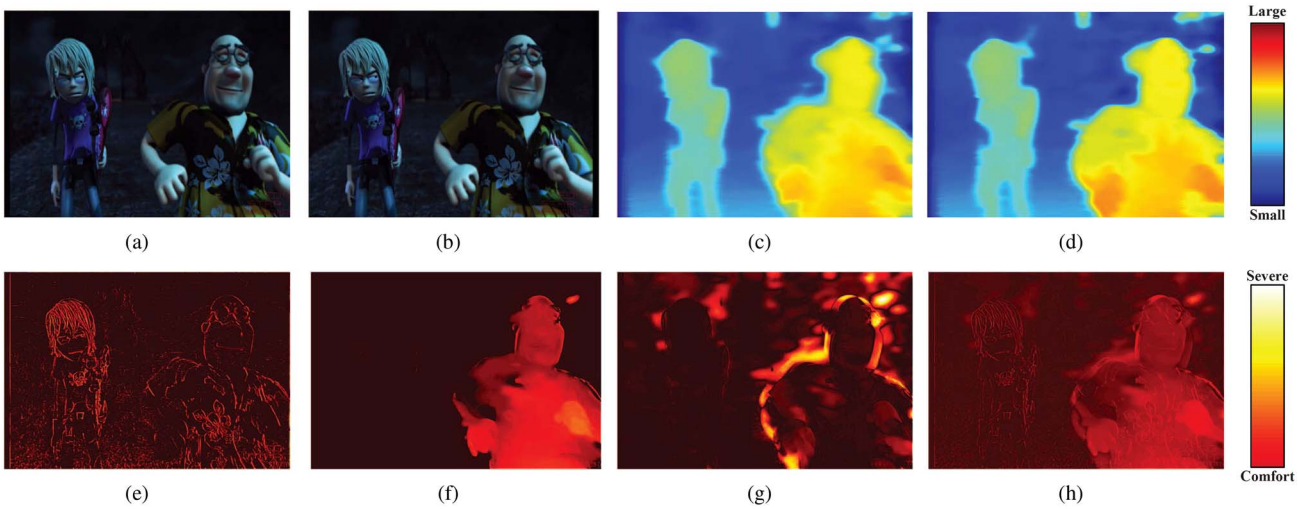

Fig. 3. (a) Left image. (b) Right image. Left disparity maps of (c) current frame and (d) next frame. Index maps of (e) spatial frequency ($f_1(\mathbf{p})$), (f) disparity magnitude ($f_2(\mathbf{p})$), (g) disparity motion ($f_3(\mathbf{p})$), and (h) their combined visual fatigue map ($F(\mathbf{p})$). For effective expression of the fatigue region, $f_1(\mathbf{p})$, $f_2(\mathbf{p})$, $f_3(\mathbf{p})$, and $F(\mathbf{p})$ are represented as reversed values.

where I and V are the inter-ocular distance and the viewing distance, respectively. Finally, the angular disparity $d_a(\mathbf{p})$ is computed as follows:

$$\begin{aligned} d_a(\mathbf{p}) &= \alpha - \beta \\ &= 2 \cdot \left\{ \tan^{-1}\left(\frac{I/2}{V}\right) - \tan^{-1}\left(\frac{I/2}{V-Z}\right) \right\}. \end{aligned} \tag{6}$$

c) Disparity motion: If the moving object has high velocity, the fusion ability of human eyes cannot follow the speed of object movement [8], [9]. That is, motion in depth with high velocity can cause visual fatigue. We exploit the disparity motion for visual fatigue prediction, and it is represented as follows:

$$M(\mathbf{p}) = \left| d_a^t(\mathbf{p}) - d_a^{t+1}(\mathbf{p}) \right|, \tag{7}$$

where $d_a^t(\mathbf{p})$ and $d_a^{t+1}(\mathbf{p})$ are the disparity values of $\mathbf{p}$ in $t-$ and $(t+1)-th$ frame, respectively.

2) Visualization and Scoring:

a) Visual fatigue map generation: A visual fatigue map is presented to show the degree of fatigue of the three visual fatigue models in a local manner efficiently. First, phase congruency is represented as follows:

$$f_1(\mathbf{p}) = \overline{PC}(\mathbf{p}), \tag{8}$$

where $\overline{PC}(\mathbf{p}) = 1 - PC(\mathbf{p})$. That is, each pixel has lower values as visual fatigue is predicted to be severe. Fig. 3(e) shows that the highly-textured region is predicted to be more discomfortable, which is extracted from the original image in Fig. 3(a). Second, based on the angular disparity information, the index map for the disparity magnitude $f_2(\mathbf{p})$ is computed as follows:

$$f_2(\mathbf{p}) = \begin{cases} 1 & |d_a(\mathbf{p})| \le \sigma_{comfort} \\ \exp\left(\sigma_{comfort} - |d_a(\mathbf{p})|\right) & otherwise \end{cases}. \tag{9}$$

If $|d_a(\mathbf{p})|$ is smaller than $\sigma_{comfort}$, $f_2(\mathbf{p})$ becomes 1, which means that the degree of fatigue is predicted to be comfortable. Otherwise, $f_2(\mathbf{p})$ gets closer to zero as $|d_a(\mathbf{p})|$ becomes larger to penalize the discomfortable region. The threshold of the comfort zone $\sigma_{comfort}$ is set to 1 degree (60 *arcmin*) [23]. With an original stereo pair as shown in Fig. 3(a) and (b), the disparity magnitude is estimated. The degree of fatigue is then predicted to be more severe as disparity magnitude becomes larger as shown in Fig. 3(f). Finally, disparity motion is represented as follows:

$$f_3(\mathbf{p}) = \exp(-M(\mathbf{p})). \tag{10}$$

By computing the difference between a current and next frame presented in Fig. 3(c) and (d), the disparity motion is obtained. In Fig. 3(g), the region with high disparity motion showed severe degree of fatigue. Based on the three index maps computed in (8)–(10), we can obtain a visual fatigue map as follows:

$$F(\mathbf{p}) = \frac{\alpha_0 + \sum_{i=1}^{3} \alpha_i f_i(\mathbf{p})}{\sum_{j=0}^{3} \alpha_j}. \tag{11}$$

Rather than a uniform composition of three predicted models, it is more effective to compute the most efficient coefficients α_0, α_1, α_2, and α_3 by multiple linear regression with the subjective evaluation results, which will be explained in Section IV-A. As shown in Fig. 3(h), the visual fatigue map is obtained by combining three index maps with optimal proportion.

b) Visual fatigue pooling: It has been stated that the worst local quality region affects the overall subjective perception significantly [31]. Therefore, we exploit $\varepsilon\% - th$ percentile pooling to compute the overall degree of fatigue as follows [31]:

$$S = \frac{1}{N_\varepsilon} \sum_{\mathbf{q} \in \Theta_i} F(\mathbf{q}), \tag{12}$$

where Θ_i denotes a set of $\varepsilon\%$ of the overall pixels scored high degree of fatigue, and N_ε is the number of pixels in Θ_i. Thus, the score S becomes higher as the image is predicted to be more comfortable, and *vice versa*.

C. Nonlinear Disparity Remapping

In this section, the proposed disparity remapping scheme is presented as two cases as shown in Fig. 4. Disparity range is determined based on the overall fatigue score in (12). Then, a remapping operator is non-linearized to alleviate visual fatigue by leveraging the visual fatigue map in (11). The depth coherence problem in a stereoscopic video is also addressed.

1) Disparity Range Adaptation: The disparity range of a stereoscopic video is predetermined in the production step. Thus, the 3D effect might be excessive or deficient according to the viewing environment and video characteristics. In order to handle this problem, we propose a disparity range adaptation method which controls the disparity range according to the degree of fatigue as shown in Fig. 4(b). By using the predicted overall fatigue score, the target disparity range R_{target} is generated as follows:

$$R_{target} = \frac{S}{\sigma} \cdot R_{comfort}. \tag{13}$$

$R_{comfort}$ denotes the difference between the maximum and minimum disparity of the predefined comfortable range, which is set to 1. In this manner, if S is smaller than σ, target disparity range becomes smaller than the $R_{comfort}$, and *vice versa*. Then, maximum and minimum disparities of R_{target}, $\bar{k}_{\max}$ and $\bar{k}_{\min}$, are computed as follows:

$$\begin{aligned} \bar{k}_{\max} &= \frac{k_{\max}}{k_{\max} - k_{\min}} \cdot R_{target} \\ \bar{k}_{\min} &= \frac{k_{\min}}{k_{\max} - k_{\min}} \cdot R_{target}, \end{aligned} \tag{14}$$

where $k_{\max}$ and $k_{\min}$ are the maximum and minimum disparities of the original disparity range, respectively.

2) Operator Nonlinearization: Although the 3D effect can be adapted by linearly remapping an input video within the determined disparity range in (14), an additional effect can be achieved by performing the operator non-linearization. Human eyes become strained when seeing stereoscopic scene which includes multiple objects with large disparity difference, *i.e.*, disparity gradient [2], [3]. In order to alleviate this problem, the remapping operator compresses the disparity gradient within the problematic region to reduce visual fatigue, while stretching the disparity gradient of a comfortable region as shown in Fig. 4(c).

By assuming that the disparity values are similar in the same object, the degree of fatigue in each object can be inferred by computing an average of the fatigue score for each disparity as follows:

$$\psi(k) = \frac{1}{N_k} \sum_{\mathbf{p} \in \Omega} (F(\mathbf{p}) \cdot \delta(d_c(\mathbf{p}) = k)), \tag{15}$$

where N_k denotes the number of pixels which have disparity $k \in [\bar{k}_{\min}, \bar{k}_{\max}]$. Then, the remapping operator can be generated as follows:

$$\phi(k) = \sum_{l=\bar{k}_{\min}}^{k} \psi(l). \tag{16}$$

After the remapping operator in (16) is applied to the original disparity map, it can be achieved that the output disparity gradient of problematic region is compressed while that of comfortable region becomes stretched as shown in Fig. 4. Note that the nonlinear disparity remapping operator prevents the disparity inversion since $\phi(k)$ is a monotonically increasing function, *i.e.*, $\phi(k) = \phi(k-1) + \psi(k)$ with $\psi(k) \geq 0$, thus $\phi(k) \geq \phi(k-1)$ for $k \geq 1$.

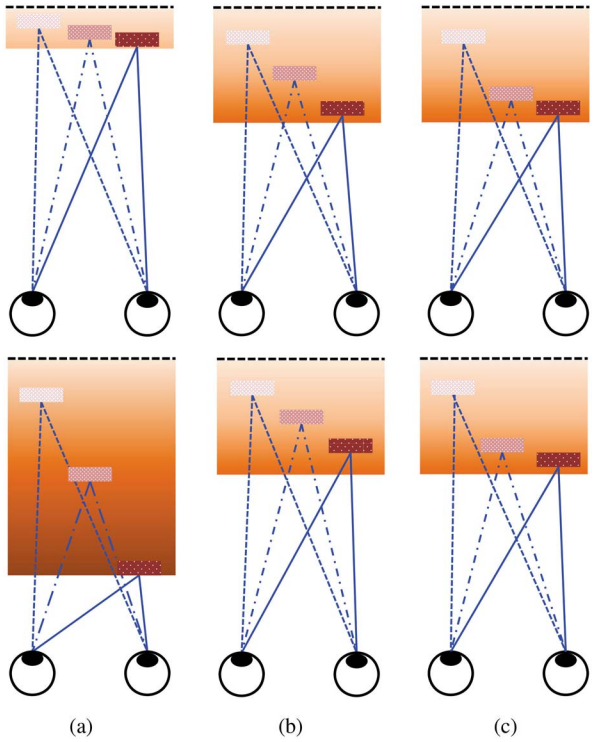

Fig. 4. Toy examples of the nonlinear disparity remapping scheme: (from top to bottom) comfortable and discomfortable cases. (a) Original sequence. Effect of (b) disparity range adaptation and (c) operator nonlinearization. Note that darker object gives more discomfort. First, disparity range is automatically adapted by considering visual fatigue and relative distances among objects are nonlinearly controlled to compress disparity gradient between discomfortable objects.

3) Temporally Coherent Disparity Remapping Operator Generation: When the disparity remapping scheme is applied to the video, it is important to consider the depth coherence between frames. If the remapping operator is independently generated in each frame, the disparity of same object in different frames may not be similar and it might cause visual artifacts. In order to solve this problem, the disparity remapping operator is generated for each scene, not a frame. In general, each scene consists of similar frames, *i.e.*, the objects and their depth distribution do not change hugely. Thus, the disparity range is determined for each scene by considering the degree of fatigue over all frames in the scene S_{scene}, which prevents the visual artifacts in retargeted frames.

Similar to the disparity range adaptation in (13), disparity range is determined as follows:

$$R_{target} = \frac{S_{scene}}{\sigma} \cdot R_{comfort}. \tag{17}$$

Also, the maximum and minimum disparity of the scene are computed as in (14). Then, an average of the fatigue score for

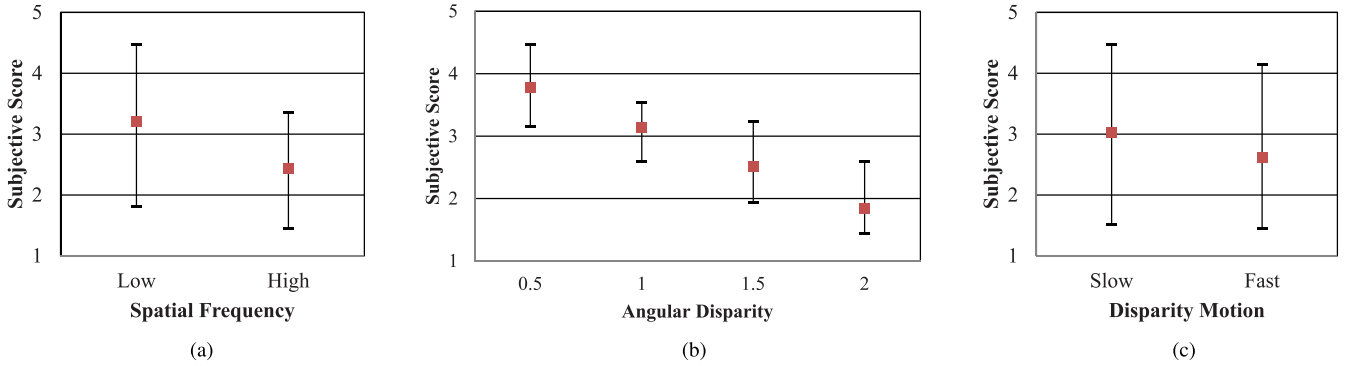

Fig. 5. MOSs for (a) spatial frequency, (b) disparity magnitude, and (c) disparity motion. The visual fatigue becomes severe in high-textured, large disparity, and fast motion videos.

each disparity is computed as follows:

$$\psi_{scene}(k) = \frac{1}{N(\Phi_s)} \sum_{t \in \Phi_s} \left(\psi^t(k)\right), \tag{18}$$

where Φ_s and $N(\Phi_s)$ denote a set of frames within the scene and the total number of frames, respectively. $\psi^t(k)$ denotes $\psi(k)$ for $t-th$ frame. Then, the remapping operator is nonlinearized as follows:

$$\phi_{scene}(k) = \sum_{l=\tilde{k}_{\min}}^{k} \psi_{scene}(l). \tag{19}$$

IV. Experimental Results

A. Analysis of Visual Fatigue Factors

A subjective evaluation was conducted to verify the validity of the selected visual fatigue factors. A 55-inch stereoscopic display was used and the viewing distance was set to 1.9m [32]. Ten subjects, from twenty five to thirty years old, participated in this subjective evaluation. All of them are experts without stereo blindness, color blindness, or low vision. Optical corrections were allowed during the experiment. Nothing is noticed about the video except warning that it might give fatigue to their eyes.

In order to obtain the most efficient coefficients in (11), the multiple linear regression was exploited between visual prediction scores and subjective evaluations of the test videos. In (12), ε is set to 10 % for the percentile pooling. The computer graphics tool (3Ds Max) was used to generate the test video sets with varying conditions. The angular disparities were distinguished into four cases: 0.5, 1.0, 1.5, and 2.0 degree. The disparity motion and image texture were divided into two cases such as fast/slow and high/low, respectively. Thus, 16 stereoscopic videos were rendered for the multiple regression. The mean opinion scores (MOSs) were obtained to measure the visual fatigue by the subjective evaluation. Without any reference video, a modified version of the single stimulus method was used to assess the level of the visual fatigue using the simple questionnaire categorized into 5 labels: "1: Severe fatigue," "2: Fatigue," "3: Moderate," "4: Comfortable," and "5: Very comfortable" [32]. The continuous ratings of all subjects were averaged for observing the tendency of the degree

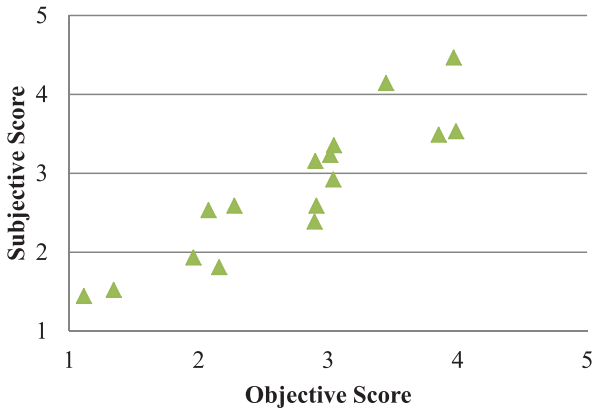

Fig. 6. Scatter plot of overall fatigue scores versus MOSs. The Pearson correlation coefficient is 0.977.

TABLE I
Multiple Linear Regression Coefficients

Coefficients	α_0	α_1	α_2	α_3
Values	0.171	3.505	5.724	0.659

fatigue of each factor. The minimum, maximum, and average MOSs of each case are presented in Fig. 5. As shown in Fig. 5(a), the MOSs (red squares) for "Low" and "High" textured videos are 3.207 and 2.432, respectively. In case of disparity magnitude as shown in Fig. 5(b), the MOSs of 0.5, 1.0, 1.5, and 2.0 degree decreased as 3.781, 3.133, 2.522, and 1.842, respectively. Finally, as in Fig. 5(c), the MOSs for "Slow" and "Fast" are 3.019 and 2.619, respectively. As a result, the degree of visual fatigue becomes high in high-textured, large disparity, and fast motion videos, which coincides well with our assumption. By exploiting the multiple regression with the MOSs and computed overall fatigue score, regression coefficients were computed as shown in Table I.

In order to see the effectiveness of the multiple linear regression, we computed the correlation between a subjective evaluation and a final fatigue score using other stereoscopic video sets. Scatter plots of the subjective MOSs versus predicted scores computed by (12) are shown in Fig. 6. In the experiment, the Pearson correlation coefficient is 0.977.

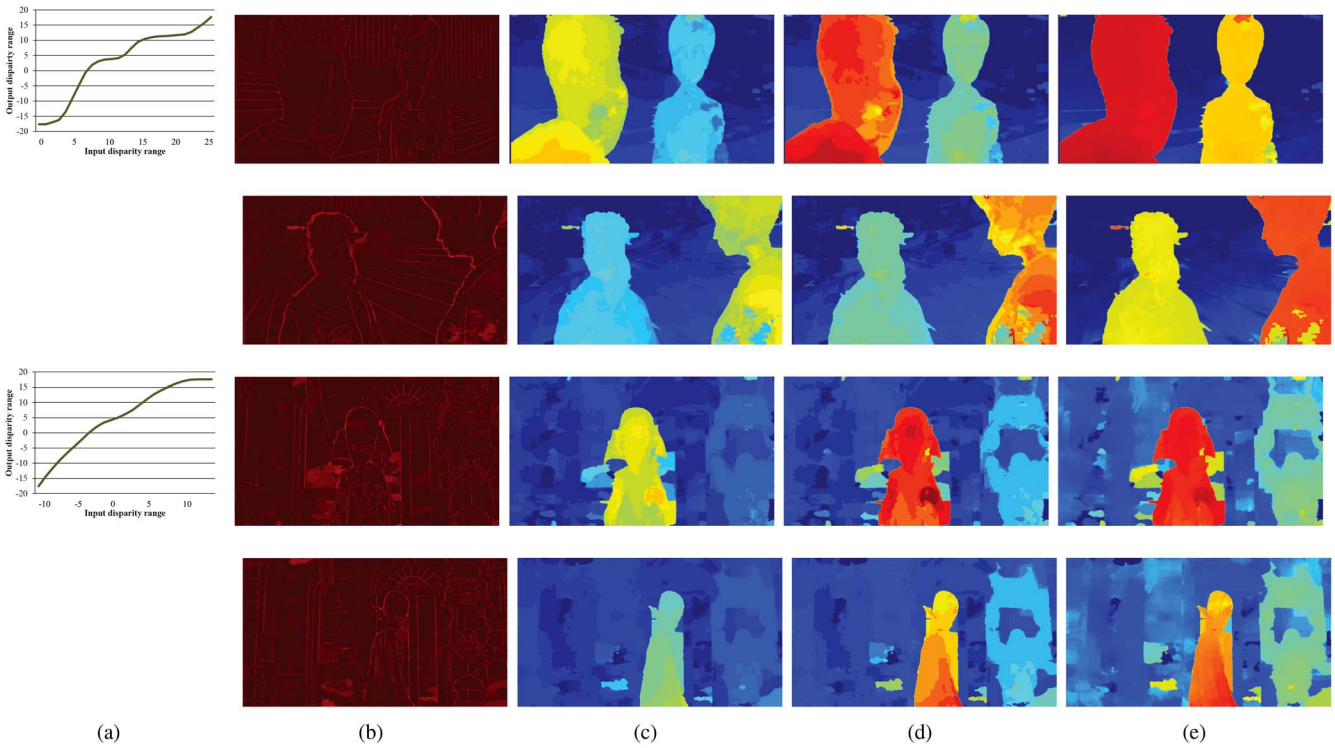

Fig. 7. Disparity remapping results of comfortable video. (a) Computed disparity remapping operator. (b) Visual fatigue map. (c) Original disparity map. (d) Linearly remapped disparity map. (e) Nonlinearly remapped disparity map. Noting that bright regions in (b) indicate that the visual fatigue is predicted to be severe, disparity range is stretched in (e) with compressing the disparity gradient of problematic regions.

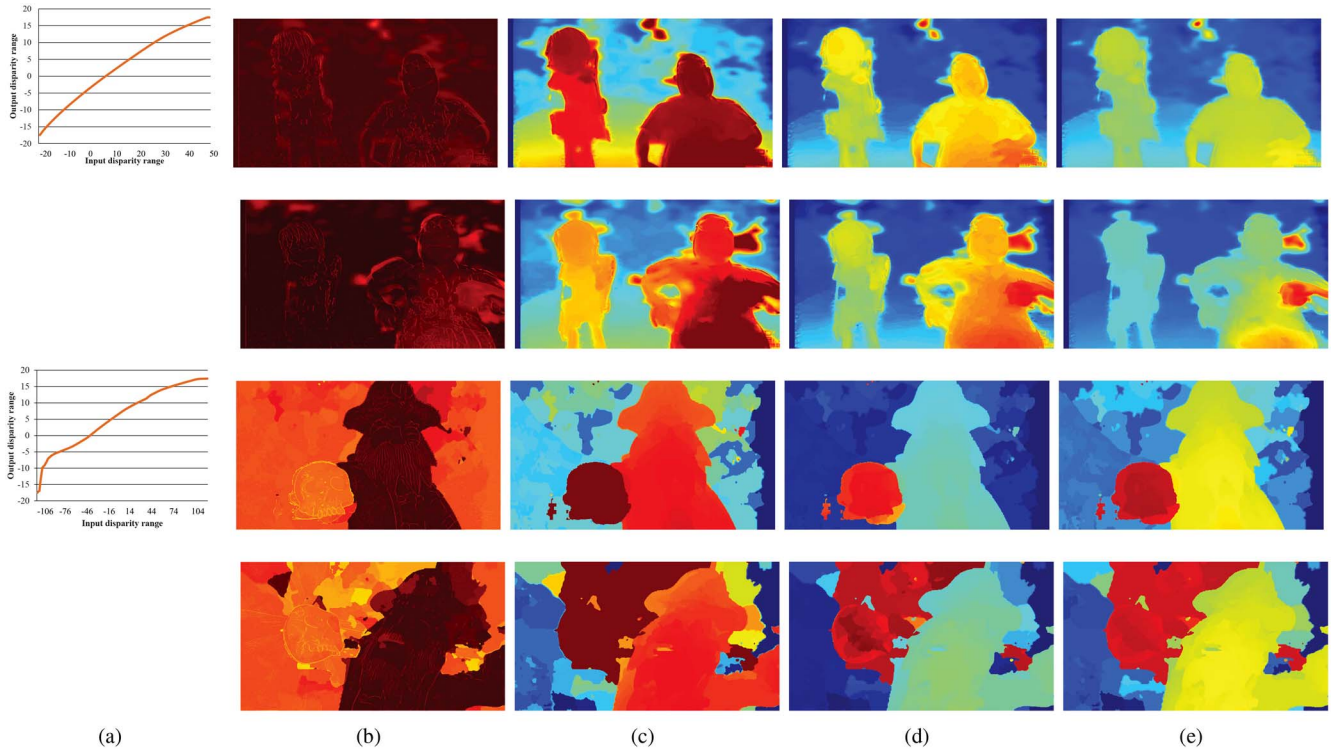

Fig. 8. Disparity remapping results of discomfortable video. (a) Computed disparity remapping operator. (b) Visual fatigue map. (c) Original disparity map. (d) Linearly remapped disparity map. (e) Nonlinearly remapped disparity map. Noting that bright regions in (b) indicate that the visual fatigue is predicted to be severe, disparity range is stretched in (e) with compressing the disparity gradient of problematic regions.

B. Nonlinear Disparity Remapping

In order to estimate disparity between stereo images, a local stereo matching method was adopted [33], [34]. Local methods are mainly composed of three steps: matching cost computation, cost aggregation and disparity computation. In experiments, the truncated absolute difference and census

Fig. 9. View synthesis results of comfortable video. (a) Visual fatigue map and an anaglyph image of (b) original video, (c) linear remapped video, and (d) nonlinear remapped video with the proposed remapping scheme. The overall disparity range is stretched, and the relative disparity in problematic regions are compressed. For effective comparison, please refer the results in Fig. 7.

transform were used to compute the matching cost [33], and the adaptive weight scheme was used in cost aggregation [34]. The sub-pixel enhancement method was applied to improve the accuracy of the estimated disparity map [35], where the quadratic polynomial interpolation was performed to reduce the errors caused by the discrete quantization of the disparity map. When an image disparity was converted to an angular disparity as in (4)–(6), inter-ocular distance I was set to 6.5cm.

A threshold in (17) was set to 0.7, which determines the degree of the fatigue for viewing condition of the input video. Remapping results of comfortable and discomfortable cases are presented in Figs. 7 and 8, respectively. Based on the average fatigue score for each disparity in (18), a disparity remapping operator was generated as shown in Figs. 7(a) and 8(a). In Fig. 7(a), disparity range is stretched since the video is determined to be comfortable, which can be interpreted that a 3D effect is low. Such results can be seen by comparing Fig. 7(c) and (d). On the other hand, in the discomfortable video as shown in Fig. 8, the disparity range is compressed to reduce the visual fatigue.

In order to observe an effect of the nonlinear remapping, it was compared with the linear remapping. Note that the same disparity range is allocated to both linear and nonlinear remapping, which is computed by the "disparity range adaptation." By comparing Fig. 7(d) and (e) with consideration for the visual fatigue map in Fig. 7(b), the disparity gradient of the fatigue region is compressed while that of the comfortable region is stretched. Also, the same effect is shown in Fig. 8(d) and (e).

C. Image Rendering

In order to verify the performance of the proposed disparity remapping scheme, a DIBR technique was used to render virtual views using the remapped disparity maps [27]. With the rendered stereo sequence, subjective evaluations were conducted. For evaluating an effect of the disparity range adaptation and nonlinear operator generation, we compared three types of stereoscopic videos: original video, linearly remapped video with an adapted disparity range, and nonlinearly remapped video. Note that the performance of the proposed disparity range adaptation method can be evaluated by comparing the original video with the linearly remapped video. Also, the performance of nonlinear remapping can be evaluated by observing the results rendered by the linear and non-linear operators.

The comparative results are presented in Figs. 9 and 10 which show the cases of comfortable and discomfortable scenes, respectively. Stereoscopic images are visualized as red(left)-cyan(right) anaglyph images. In the comfortable scene, it can be seen that the disparity range becomes larger than the original one by comparing Fig. 9(b) and (c). Also, the difference between linear and nonlinear remapping results can be observed by comparing the results of Fig. 9(c) and (d).

Fig. 10. View synthesis results of discomfortable video. (a) Visual fatigue map and an anaglyph image of (b) original video, (c) linearly remapped video, and (d) nonlinearly remapped video with the proposed remapping scheme. The overall disparity range and the relative disparity in problematic regions are compressed. For effective comparison, please refer the results in Fig. 8.

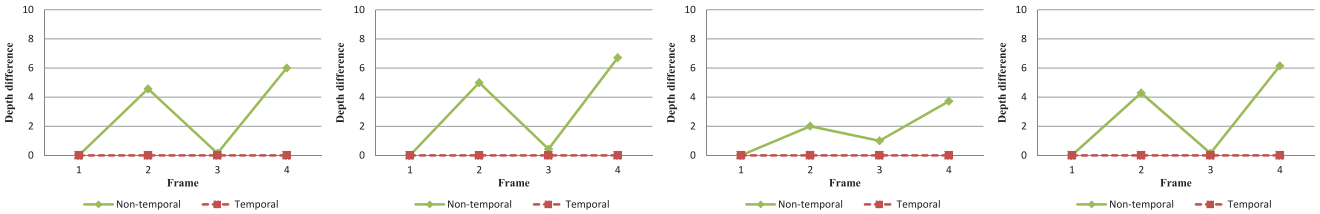

Fig. 11. Depth differences between corresponding points in the consecutive frames. Horizontal axis denotes the tth frame and its value is presented by the difference of tth and $(t+1)$th frame. The proposed remapping scheme allocates same depth value for corresponding points, which reduces flickering artifacts in the rendered video.

Considering the visual fatigue map presented in Fig. 9(a), the disparity gradient of fatigue region is more compressed in the proposed method as shown in Fig. 9(d). The example of discomfortable sequence is shown in Fig. 10. By comparing Fig. 10(b) with Fig. 10(c) and (d), the disparity range becomes compressed by the results of the disparity range adaptation. Furthermore, the proposed nonlinear disparity remapping shows disparity gradient compression in problematic regions.

In order to verify that the proposed remapping scheme improves temporal coherency, depth difference between corresponding points of adjacent frames were computed. We extracted four points in the first frame, and computed the difference of depth values of their corresponding points in the next frame. As shown in Fig. 11, depth fluctuation occurs when the remapping operator is generated for each frame. However, it is shown that the depth fluctuation is not observed by generating the remapping operator for each scene.

Subjective assessments were conducted to evaluate the degree of fatigue and depth sensation among original, linearly remapped, and nonlinearly remapped sequence. In the assessment, seven subjects were participated in and a modified Double Stimulus Continuous Quality Scale (DSCQS) methods was used [36]. The DSCQS method compares the scores between reference and re-produced videos. The original video was selected to the reference and the linearly and nonlinearly remapped videos were set to test videos. Four comfortable and discomfortable videos were used as demo videos, respectively, and running time of each video is around 4 to 15 seconds. The subjects were instructed to watch the original and re-produced video repetitively twice times, and graded the degree of fatigue and the depth sensation of both videos. The level of visual fatigue is divided into five scales: "1: Severe fatigue," "2: Fatigue," "3: Moderate," "4: Comfortable," and "5: Very comfortable." Also, the level of depth sensation is divided into

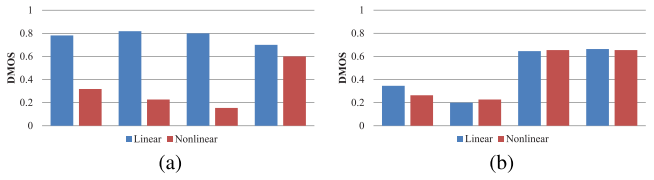

Fig. 12. DMOSs for (a) visual fatigue and (b) depth sensation in comfortable videos. Since the disparity range is stretched by the disparity range adaptation, both visual fatigue and depth sensation increase. However, the proposed scheme shows more comfortable results than the linear remapping since an operator is nonlinearized to relax the visual fatigue.

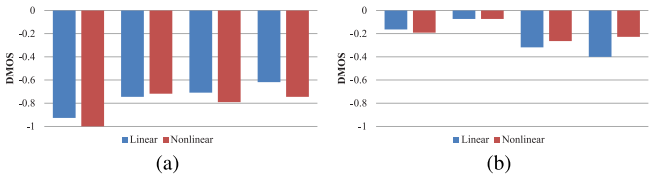

Fig. 13. DMOSs for (a) visual fatigue and (b) depth sensation in discomfortable videos. Since disparity range is compressed, both visual fatigue and depth sensation increase. The proposed scheme shows more comfortable results than linear remapping. It can be seen that the operator nonlinearization in the proposed method relaxes the visual fatigue.

five scales: "1: Very high," "2: High," "3: Medium," "4: Low," and "5: Very low." Fig. 12 shows the Different Mean Opinion Score (DMOS) results of comfortable videos. Note that the DMOS is obtained by subtracting the MOS of a remapped video from that of an original video. The DMOSs of the degree of fatigue and depth sensation are positive, which indicates that the degree of fatigue and depth sensation increase in both cases. Since the disparity range is stretched, the subject might feel more fatigue in the re-produced cases. However, as shown in Fig. 12(a), it can be seen that subjects felt less fatigue in the nonlinearly remapped videos. It shows that the nonlinearly remapped videos give less fatigue than the one from the linearly remapped videos. In addition, as shown in Fig. 12(b), depth sensation of comfortable videos similarly increases in both cases. In contrast to this, as shown in Fig. 13, the DMOSs of linearly and nonlinearly remapped videos are all negative, which means that the results of both methods show much comfort than the original videos. In addition, depth sensation decreases in both cases. In Fig. 13(a), the DMOSs of the nonlinear results are higher than those of the linear results. That is, the subjects felt less fatigue in the nonlinear cases. Since the disparity ranges are compressed in discomfortable videos, the depth sensation decreases in linear and nonlinear cases of each video as shown in Fig. 13(b). Unlike the DMOSs for the visual fatigue in comfortable videos (Fig. 12(a)), those in discomfortable videos show small differences between the linear and the nonlinear cases (Fig. 13(a)). It can be seen that the disparity range adaptation is more dominant process than the operator non-linearization in reducing the visual fatigue in discomfortable videos. In order to verify the reliability of DMOSs results, statistical significance is verified. As shown in Tables II and III, the improvements in the visual fatigue and the depth sensation are statistically significant for both comfortable and discomfortable cases. Note that the result is statistically significant if p-value is less than 0.05 [38].

TABLE II
STATISTICAL RESULTS IN COMFORTABLE VIDEOS

	Visual fatigue		Depth sensation	
Method	**Linear**	**Nonlinear**	**Linear**	**Nonlinear**
Mean of DMOS	0.775	0.325	0.464	0.450
Standard error of the mean	0.354	0.424	0.314	0.346
p-value	$p < 0.001$	$p < 0.001$	$p < 0.001$	$p < 0.001$

TABLE III
STATISTICAL RESULTS IN DISCOMFORTABLE VIDEOS

	Visual fatigue		Depth sensation	
Method	**Linear**	**Nonlinear**	**Linear**	**Nonlinear**
Mean of DMOS	−0.75	−0.813	-0.239	-0.189
Standard error of the mean	0.309	0.335	0.297	0.364
p-value	$p < 0.001$	$p < 0.001$	$p < 0.001$	$p = 0.001$

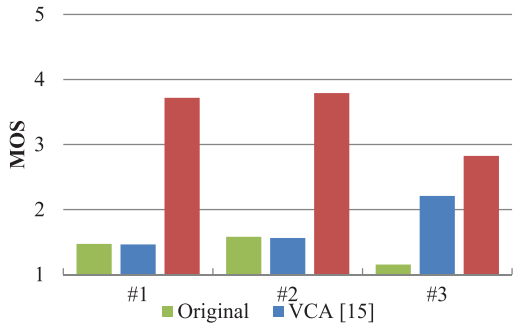

Fig. 14. MOSs for the visual fatigue in the three video sequences. The proposed scheme provides more comfortable results than the VCA.

D. Comparison With State-of-the-Art Method

We compared the proposed method with state-of-the-art method for visual fatigue relaxation: the visual comfort amelioration (VCA) [15]. Note that the proposed method also controls depth sensation while the VCA aims at reducing visual fatigue only. In (17), the disparity range is stretched when an input video is considered as comfortable, and *vice versa*. Thus, the experiments were presented to compare the performance of reducing visual fatigue. Each of two methods was applied to three video sequences, and a subjective evaluation was then performed in terms of the visual fatigue.

As shown in Fig. 14, the proposed method relaxes the visual fatigue effectively. In the video sequences 1 and 2, the rendered results of the VCA are generated without any remapping process. That is, the VCA does not perform the disparity remapping process, since these video sequences are predicted to be comfortable (the degree of the visual fatigue is low). In contrast to this, they are predicted to be discomfortable in the proposed method, generating (re-rendered) visually comfortable video sequences. In the video sequence 3, both the VCA and the proposed method consider this video sequence as discomfortable, which remaps the original disparity to reduce the visual fatigue. We can find that the proposed method relaxes the visual fatigue more effectively than the VCA. The reliability of the MOSs results was evaluated as in Table IV, which shows that the MOSs results are statistically significant.

The VCA aims to generate a disparity remapping operator in stereoscopic images. When the VCA is applied to a

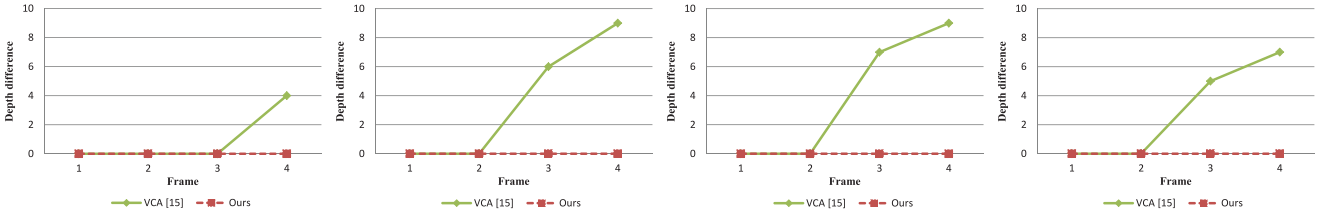

Fig. 15. Depth differences between corresponding points in the consecutive frames. The horizontal axis denotes the tth frame and its value is computed by the difference of tth and $(t+1)$th frame. The proposed remapping scheme allocates the same depth value for corresponding points, while the VCA gives incoherent depth remapping results.

TABLE IV
STATISTICAL RESULTS IN DISCOMFORTABLE VIDEOS

	Visual fatigue		
Method	**Original**	**VCA [15]**	**Ours**
Mean of MOS	1.403	1.745	3.561
Standard error of the mean	0.263	0.301	0.376
p-value	$p < 0.001$	$p < 0.001$	$p < 0.001$

stereoscopic video, the disparity remapping operator is generated independently at each frame. Thus, the depth values of the corresponding region may change. To verify the temporal fluctuation, we extracted four points in the reference frame and observed the changes of the depth values of their corresponding points at each frame. As shown in Fig. 15, the VCA shows depth fluctuation while the proposed method allocates the same depth values to the corresponding points.

V. CONCLUSION

A nonlinear disparity remapping scheme has been presented to reduce visual fatigue in a stereoscopic video. The visual fatigue was predicted by modeling three fatigue inducing factors: spatial frequency, disparity motion, and disparity magnitude. A visual fatigue map was extracted, and an overall fatigue score was computed by the pooling strategy. To generate nonlinear remapping operator, disparity range was adapted by the overall fatigue score of the scene. Then, with a given visual fatigue map, remapping operator was non-linearized by compressing the disparity gradient of a problematic region. The experimental results showed that the disparity range is adapted with respect to the overall fatigue score, which gives a reduced 3D effect to the discomfortable scene and *vice versa*. It was shown that the visual fatigue is reduced by non-linearizing the remapping operator. Also, the proposed method was compared with the state-of-the-art method. The proposed method has a following limitation. Since it is assumed that an object in stereoscopic video has similar disparity, the proposed method gives distorted results if the object has in-depth-motion. In further research, we will leverage the just noticeable depth difference concept in the nonlinear disparity remapping scheme [13]. Also, an importance based disparity remapping scheme [10] can be combined with our method.

ACKNOWLEDGMENT

The authors would like to thank Dr. H. Sohn, S.-I. Lee, and Prof. Y. M. Ro for their considerate assistance in generating the comparative experimental results.

REFERENCES

[1] L. Chauvier, K. Murray, S. Parnall, R. Taylor, and J. Walker, "Does size matter? The impact of screen size on stereoscopic 3DTV," in *Proc. Int. Bridge Conf. (IBC)*, 2010, pp. 1–14.
[2] D. M. Hoffman, A. R. Girshick, K. Akeley, and M. S. Banks, "Vergence-accommodation conflicts hinder visual performance and cause visual fatigue," *J. Vis.*, vol. 8, no. 3, pp. 1–30, 2008.
[3] M. Lambooij, W. IJsselsteijn, M. Fortuin, and I. Heynderickx, "Visual discomfort and visual fatigue of stereoscopic displays: A review," *J. Imag. Sci. Technol.*, vol. 53, no. 3, May 2009, Art. ID 30201.
[4] M. Wöpking, "Viewing comfort with stereoscopic pictures: An experimental study on the subjective effects of disparity magnitude and depth of focus," *J. Soc. Inf. Display*, vol. 3, no. 3, pp. 101–103, Dec. 1995.
[5] D. Kim and K. Sohn, "Visual fatigue prediction for stereoscopic image," *IEEE Trans. Circuits Syst. Video Technol.*, vol. 21, no. 2, pp. 231–236, Feb. 2011.
[6] J. Choi, D. Kim, S. Choi, and K. Sohn, "Visual fatigue modeling and analysis for stereoscopic video," *Opt. Eng.*, vol. 51, no. 1, Feb. 2012, Art. ID 017206.
[7] S. Yano, M. Emoto, and T. Mitsuhashi, "Two factors in visual fatigue caused by stereoscopic HDTV images," *Displays*, vol. 25, no. 4, pp. 141–150, Nov. 2004.
[8] F. Speranza, W. Tam, R. Renaud, and N. Hur, "Effect of disparity and motion on visual comfort of stereoscopic images," *Proc. SPIE Stereoscop. Displays Virt. Real. Syst.*, vol. 6055, pp. 94–103, 2006, Art. ID 60550B.
[9] Y. J. Jung, S. Lee, H. Sohn, H. W. Park, and Y. M. Ro, "Visual comfort assessment metric based on salient object motion information in stereoscopic video," *J. Electron. Imag.*, vol. 21, no. 1, Feb. 2012, Art. ID 011008.
[10] M. Lang *et al.*, "Nonlinear disparity mapping for stereoscopic 3D," *ACM Trans. Graph.*, vol. 29, no. 4, Jul. 2010, Art. ID 75.
[11] C. Wu, C.-T. Li, Y.-C. Lai, C.-C. Cheng, and L.-G. Chen, "Disparity remapping by nonlinear perceptual discrimination," in *Proc. 3D Syst. Appl.*, Seoul, Korea, 2011, pp. 342–346.
[12] H.-S. Lin, S.-H. Guan, C.-T. Lee, and M. Ouhyoung, "Stereoscopic 3D experience optimization using cropping and warping," in *Proc. ACM SIGGRAPH Asia Sketches*, Hong Kong, 2011, Art. ID 40.
[13] S.-W. Jung and S.-J. Ko, "Depth sensation enhancement using the just noticeable depth difference," *IEEE Trans. Image Process.*, vol. 21, no. 8, pp. 3624–3637, Aug. 2012.
[14] T. Yan, R. W. H. Lau, Y. Xu, and L. Huang, "Depth mapping for stereoscopic videos," *Int. J. Comput. Vis.*, vol. 102, pp. 293–307, Mar. 2013.
[15] H. Sohn, Y. Jung, S. Lee, F. Speranza, and Y. M. Ro, "Visual comfort amelioration technique for stereoscopic images: Disparity remapping to mitigate global and local discomfort causes," *IEEE Trans. Circuits Syst. Video Technol.*, vol. 24, no. 5, pp. 745–758, May 2014.
[16] D. Kim, S. Choi, and K. Sohn, "Visual comfort enhancement for stereoscopic video based on binocular fusion characteristics," *IEEE Trans. Circuits Syst. Video Technol.*, vol. 23, no. 3, pp. 482–487, Mar. 2013.
[17] H. Yamanoue, M. Okui, and F. Okano, "Geometrical analysis of puppet-theater and cardboard effects in stereoscopic HDTV images," *IEEE Trans. Circuits Syst. Video Technol.*, vol. 16, no. 6, pp. 744–752, Jun. 2006.
[18] J. Choi, D. Kim, B. Ham, S. Choi, and K. Sohn, "Visual fatigue evaluation and enhancement for 2D-plus-depth video," in *Proc. IEEE Int. Conf. Image Process.*, Hong Kong, 2010, pp. 2981–2984.
[19] T. Shibata, J. Kim, D. M. Hoffman, and M. S. Banks, "The zone of comfort: Predicting visual discomfort with stereo displays," *J. Vis.*, vol. 11, no. 8, pp. 1–29, 2011.

[20] W. J. Tam, F. Speranza, S. Yano, K. Shimono, and H. Ono, "Stereoscopic 3D-TV: Visual comfort," *IEEE Trans. Broadcast.*, vol. 57, no. 2, pp. 335–346, Jun. 2011.
[21] M. Emoto, T. Niida, and F. Okano, "Repeated vergence adaptation causes the decline of visual functions in watching stereoscopic television," *J. Display Technol.*, vol. 1, no. 2, pp. 328–340, Dec. 2005.
[22] M. Lambooij, M. Fortuin, W. A. IJsselsteijn, B. J. Evans, and I. Heynderickx, "Susceptibility to visual discomfort of 3-D displays by visual performance measures," *IEEE Trans. Circuits Syst. Video Technol.*, vol. 21, no. 12, pp. 1913–1923, Dec. 2011.
[23] (Nov. 2014). *3D Consortium*. [Online]. Available: http://www.3dc.gr.jp/english/index.html
[24] P. Burt and B. Julesz, "A disparity gradient limit for binocular fusion," *Science*, vol. 208, no. 444, pp. 615–617, May 1980.
[25] Y. Nojiri, H. Yamanoue, A. Hanazato, and F. Okano, "Measurement of parallax distribution, and its application to the analysis of visual comfort for stereoscopic HDTV," *Proc. SPIE Stereoscop. Displays Virt. Real. Syst.*, vol. 5006, May 2003, Art. ID 195.
[26] H. Sohn, Y. J. Jung, S. Lee, and Y. M. Ro, "Predicting visual discomfort using object size and disparity information in stereoscopic images," *IEEE Trans. Broadcast.*, vol. 59, no. 1, pp. 28–37, Mar. 2013.
[27] C. Fehn, "Depth-image-based rendering (DIBR), compression and transmission for a new approach on 3D-TV," *Proc. SPIE Stereoscop. Displays Virt. Real. Syst.*, vol. 5291, pp. 93–104, May 2004.
[28] M. C. Morrone and D. C. Burr, "Feature detection in human vision: A phase-dependent energy model," *Proc. Roy. Soc. London*, vol. 235, no. 1280, pp. 221–245, Dec. 1988.
[29] L. Henriksson, A. Hyvärinen, and S. Vanni, "Representation of cross-frequency spatial phase relationships in human visual cortex," *J. Neurosci.*, vol. 29, no. 45, pp. 14342–14351, Nov. 2009.
[30] P. Kovesi, "Image features from phase congruency," *Videre J. Comp. Vis. Res.*, vol. 1, no. 3, pp. 1–26, 1999.
[31] A. K. Moorthy and A. C. Bovik, "Visual importance pooling for image quality assessment," *IEEE J. Sel. Topics Signal Process.*, vol. 3, no. 2, pp. 193–201, Apr. 2009.
[32] *Methodology for the Subjective Assessment of the Quality of Television Pictures*, ITU-R Recommendation Standard BT. 500-13, 2012.
[33] D. Scharstein and R. Szeliski, "A taxanomy and evaluation of dense two-frame stereo correspondence algorithms," *Int. J. Comp. Vis.*, vol. 47, nos. 1–3, pp. 7–42, 2002.
[34] K.-J. Yoon and I. S. Kweon, "Adaptive support-weight approach for correspondence search," *IEEE Trans. Pattern Anal. Mach. Intell.*, vol. 28, no. 4, pp. 650–656, Apr. 2006.
[35] Q. Yang, R. Yang, J. Davis, and D. Nister, "Spatial-depth super resolution for range images," in *Proc. IEEE Conf. Comput. Vis. Pattern Recogn.*, Minneapolis, MN, USA, 2007, pp. 1–8.
[36] *Subjective Assessment of Stereoscopic Television Pictures*, ITU-R Recommendation Standard BT.1438, 2000.
[37] (Nov. 2014). *3dtv.at*. [Online]. Available: http://www.3dtv.at
[38] S. D. Schlotzhauer, *Elementary Statistics Using JMP*. Cary, NC, USA: SAS, 2007.

Changjae Oh (S'13) received the B.S. and M.S. degrees in electrical and electronic engineering from Yonsei University, Seoul, Korea, in 2011 and 2013, respectively, where he is currently pursuing the Ph.D. degree. His current research interests include 3-D computer vision, 3-D visual fatigue assessment, and image segmentation.

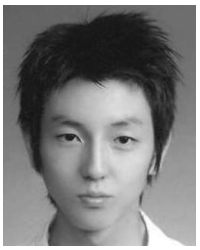

Bumsub Ham (M'14) received the B.S. and Ph.D. degrees from the School of Electrical and Electronic Engineering, Yonsei University, Seoul, Korea, in 2008 and 2013, respectively. He is currently a Post-Doctoral Research Fellow with the Willow Team of INRIA Rocquencourt, École Normale Supérieure de Paris, and Centre National de la Recherche Scientifique. His current research interests include variational methods and geometric partial differential equations, both in theory and applications in computer vision and image processing, in particular, regularization, stereovision, super-resolution, and high dynamic range imaging. He was the recipient of the Honor Prize at the 17th Samsung Human-Tech Prize in 2011 and the Grand Prize in Qualcomm Innovation Fellowship in 2012.

Sunghwan Choi (S'10) received the B.S. degree in electronic engineering and avionics from the Korea Aerospace University, Gyeonggi-do, Korea, in 2009. He is currently pursuing the joint M.S. and Ph.D. degrees in electrical and electronic engineering from Yonsei University, Seoul, Korea. His current research interests include 3-D image and video processing, computer vision, computational aspects of human vision, and image-based modeling and rendering.

Kwanghoon Sohn (M'92–SM'12) received the B.E. degree in electronic engineering from Yonsei University, Seoul, Korea, the M.S.E.E. degree in electrical engineering from the University of Minnesota, and the Ph.D. degree in electrical and computer engineering from North Carolina State University in 1983, 1985, and 1992, respectively. He was a Senior Research Staff Member at the Satellite Communication Division, Electronics, and Telecommunications Research Institute, Daejeon, Korea, from 1992 to 1993, and a Post-Doctoral Fellow at the MRI Center, Medical School of Georgetown University in 1994. He was a Visiting Professor at Nanyang Technological University from 2002 to 2003. He is currently a Professor with the School of Electrical and Electronic Engineering, Yonsei University. His research interests include 3-D image processing, computer vision, and image communication. He is a member of SPIE.